CO1-1 Quantitative Characerization of Microstructures in Steels using Small-Angle X-ray Scattering

Y. Oba, R. Inoue[1] and M. Sugiyama[1]

Materials Sciences Research Center, Japan Atomic Energy Agency
[1]Institute for Integrated Radiation and Nuclear Science, Kyoto University

INTRODUCTION: Nano- and microstructures are crucial for steels because they are closely related with the mechanical properties. Small-angle scattering (SAS) is a powerful tool to quantitatively characterize the nano- and microstructures because of its large gauge volume. Several research groups have reported the applications of SAS to steel researches [1-3].

However, model alloys having simple nanostructures are often examined by SAS to simplify the discussion. For further progress, it is necessary to apply SAS to more practical materials. Stainless steel is a typical commercial steel and has complex nanostructures. In this case, small-angle X-ray scattering (SAXS) measurements using in-house instruments is suitable as a usual characterization technique closely linked with practical materials processing. Although it takes over several hours for a SAXS measurement using the in-house SAXS instruments, steels are stable for such long measurements.

Therefore, in this study, the nanostructures in the stainless steels were investigated to confirm the ability of the in-house SAXS instrument.

EXPERIMENTS: SAXS measurements were performed using the in-house SAXS instrument with Mo $K\alpha$ radiation. For steels, conventional Cu $K\alpha$ radiation is not useful because of low transmission and high fluorescence X-ray emission. Scattering patterns were obtained using a two-dimensional detector (PILATUS 100k) equipped with a 1000 μm-thick silicon sensor to efficiently detect the high energy Mo $K\alpha$ radiation. The path of X-ray between the entrance slit and up to the detector including the sample area was evacuated to eliminate background scattering from air and vacuum windows. In this study, the original vacuum tubes were changed to thicker vacuum pipes to improve the degree of vacuum and further reduce the background scattering from residual air.

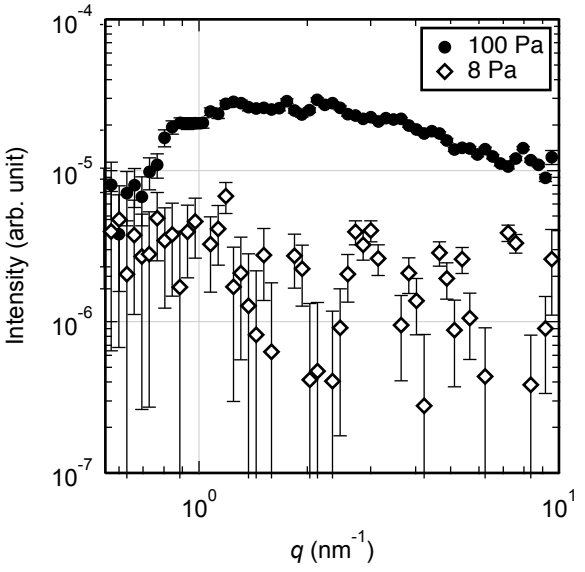

Fig. 1. Background scattering profiles.

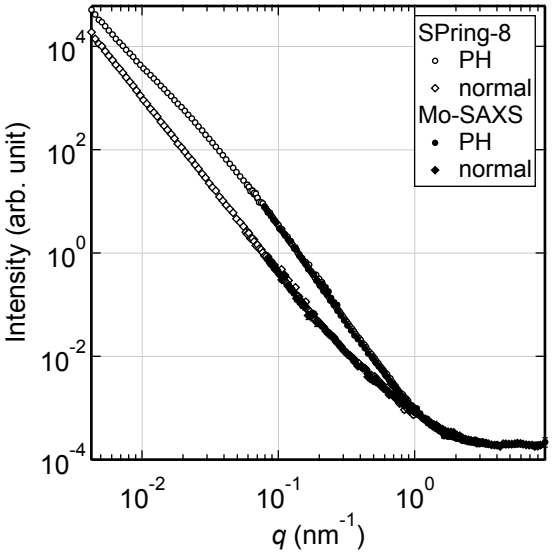

Fig. 2. Scattering profiles of stainless steels. Circles and diamonds denote precipitation hardening (PH) and normal stainless steels, respectively. Open and filled symbols are data obtained using SPring-8 and Mo-SAXS.

RESULTS: Fig. 1 shows the background scattering before and after changing the vacuum pipes. With this changing, the ultimate vacuum was improved from 100 Pa to a few Pa and the background scattering intensity decreases to about 1/10.

Fig. 2 shows the scattering profiles of precipitation hardening (PH) and normal stainless steels. Both the profiles obtained using Mo-SAXS agree well with the corresponding scattering profiles obtained using the SAXS instrument in SPring-8. The profile of the PH stainless steel has a hump at about $q < 1$ nm^{-1} compared to that of the normal stainless steel. This hump is attributed to the scattering from precipitates. Therefore, we successfully observed the precipitates in stainless steels using SAXS.

REFERENCES:

[1] M. Ohnuma *et al.*, Acta Mater., **57** (2009) 5571-5581.
[2] Y. Oba *et al.*, ISIJ Int., **51** (2011) 1852-1858.
[3] A. Deschamps *et al.*, Mater. Lett., **65** (2011) 2265-2268.

CO1-2 Fabrication of *m*=6 spuermirror on ellipsoidal metal substrate

M. Hino[1], T.Hosobata[2], T.Oda[1], H.Yoshinaga[1], S. Takeda[2], Y.Yamagata[2], H.Endo[3], N.L.Yamada[3], F. Funama[4], Y. Kawabata[1]

[1]*Institute for Integrated Radiation and Nuclear Science, Kyoto University (KURNS), Japan*
[2] *RAP, RIKEN, Japan*
[3] *IMSS, KEK, Japan*
[4]*Dept., Nucl. Eng., Kyoto University, Japan*

INTRODUCTION: Progress of neutron optical devices is very significant. Recently we proposed promising fabrication method for aspherical focusing supermirror with metal substrate [1-4]. The metallic substrate is robust and ductile, to which able to fabricate steeply curved surface with high form accuracy. It is also applicable to use under high radiation irradiation and high-temperature filed, even at a place close to the neutron target and moderator. Furthermore, it is possible to fabricate a large focusing mirror by combining multiple segmented mirrors with mechanical fastening entailing the usage of screw holes and fixture tabs. The big problem was required surface roughness for neutron mirror. The roughness should be smaller than 0.3 nm for high-*m* supermirror coating. Here *m* is the maximum critical angle of the mirror in units of critical angle of natural nickel. By using electroless nickel-phosphorus (Ni-P) plating, we overcame the problem and are establishing fabrication process for aspherical focusing supermirror. In this study, we show a latest result for neutron focusing experiment with a couple of ellipsoidal supermirrors with metallic substrates.

EXPERIMENTS: We fabricated ellipsoidal metallic substrates with the Ni-P plating, based on the technology using ultrahigh precision cutting with correction processing, followed by mechanical precision polishing. The first precise manufacturing was conducted at a CNC machine for development of neutron optical devices at workshop of the KURNS. The ultra-precise manufacturing, polishing and cleaning of the metallic substrate were conducted at RIKEN. The supermirror coating was conducted with ion beam sputtering machine at the KURNS (KUR-IBS) [5]. The neutron experiments were conducted at CN-3 beam line at the KURNS and the BL06 (VIN ROSE) beam port at J-PARC MLF [6]. We have succeeded in fabricated a couple of *m*=3 NiC/Ti ellipsoidal supermirrors in which length of 900mm [7]. The semi-major and semi-minor axes of the ellipsoidal supermirror were 1250 mm and 65.4 mm, respectively. The acceptable angle of the minor axis arc of the ellipsoidal supermirror is 20 degree. In this study, we tried to fabricate higher-*m* NiC/Ti ellipsoidal supermirrors in which substrate was same with the *m*=3 NiC/Ti one. Here the required number of layers of high-*m* supermirror increases with the proportional of m^4, in which principle is well known as Porod's law. We have fabricated *m*=5 and *m*=6 NiC/Ti supermirrors in which number of layers were 3000 and 5000, respectively.

RESULTS:
Figure 1 shows photograph of *m*=6 NiC/Ti supermirror fabricated by the KUR-IBS. As shown in Fig. 1(a), the supermirror coating itself was succeeded, however, it was not tough for temperature difference. Here one of three supermirrors peeled off as shown in Fig. 1(b). The performance of supermirrors were not so good and it is still necessary to improve fabrication process for higher-*m* ellipsoid supermirror. By using the ellipsoid supermirror, we succeeded in observation of first neutron resonance spin echo signal of focusing neutron beam at BL06 at the MLF, J-PARC [8].

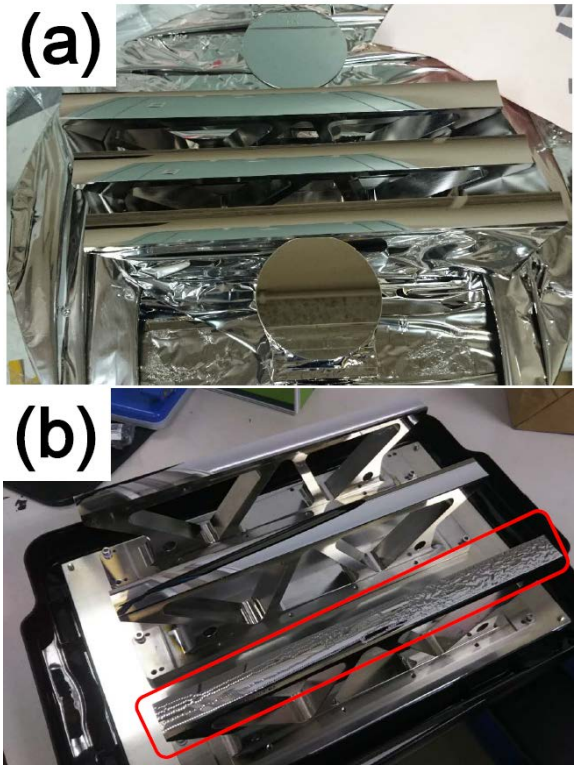

Fig. 1. Photograph of m=6 NiC/Ti supermirror coated by the KUR-IBS. (a) just after the deposition (b) after about 30° temperature change with transportation.

REFERENCES:
[1]J.Guo *et al.*, Optics Express **22** (2014) 063108.
[2]J.Guo *et al.*, Review of Scientific Instruments 86(2015) 86 (2015) 063108.
[3]S.Takeda *et al.*, Optics Express **24** (2016) 12478.
[4]T.Hosobata *et al.*, Optics Express **25** (2017) 20012.
[5]M.Hino *et al.*, Nucl. Instr. and Meth., **797** (2015) 265.
[6]M.Hino *et al.*, J. Nucl. Sci. Technol. **54** (2017) 1223.
[7]M.Hino *et al.*, KURRI Progress report 2017 CO1-8.
[8]H.Endo *et al.*, Physica B, **564** (2019) 91.

CO1-3 Character of DNA damage induced by nuclear palnt neutron beams

H. Terato, Y. Tokuyama[1], K. Mori[1], N. Osada, H. Tanaka[2] and T. Saito[2]

Advanced Science Research Center, Okayama University

[1]Analytical Research Center for Experimental Sciences, Saga University

[2]KURNS, Kyoto University

INTRODUCTION: Radiation biological effects are arrived via DNA damaging by ionizing radiation, because DNA loads genetic information. There have been a lot of studies about radiation DNA damage, and the most of them were for gamma- and X-rays' ones, but less other radiation qualities. We have studied for the DNA damage with heavy ion beams, previously [1, 2]. These studies indicated that the DNA damage with heavy ion beams were unique, indicating that a lot of clustered DNA damage were generated including DNA double strand break (DSB). Clustered DNA damage is a complex damage containing multiple lesions in the local region of DNA. This damage strongly inhibits DNA polymerization, and shows less repairable. Here, we analyze the DNA damage with neutrons from nuclear power plant to unveil the molecular mechanism of neutron biological effect. The neutron beam is also high LET radiation as same as heavy ion beam. Therefore, we will find some interesting character of DNA damage with neutron like heavy ion beam.

EXPERIMENTS: Cultured cells of Chinese hamster ovary (CHO) AA8 strain were irradiated with neutron beams in the Kyoto University Reactor. The cells were cultivated with the conventional method. The logarithmic growing cells were recovered by trypsinization, and set into a polypropylene tube for irradiation. The irradiation time was up to three hours with sampling in every 30 minutes. The estimated dose rate of neutron was 1Gy h^{-1}. After irradiation, the cells were immediately frozen by dry ice, and stored until analysis. The procedures of DNA damage analysis were mass spectrometry and electrophoresis for base damage and strand break, respectively [2 – 4]. For base damage analysis, we focused on the oxidative base damage, that is common damage with ionizing radiation. The chromosomal DNA were extracted from the irradiated cells, and were digested by nuclease to obtain the separated nucleotide units. Then, the nucleotide mixture was analyzed by mass spectrometry. For DSB analysis, the irradiated cells were embedded into low-melting agarose plug just after irradiation. The plugs were digested by protease and then electrophored. The sheared chromosomal DNA are released from the gel plug in electrophoresis gel, but the intact ones stay in the plug. The gel was stained by ethidium bromide, and the DNA bands were visualized. We compared the staying and released DNA bands for DNA shearing by neutron beams.

RESULTS: The result for base damage indicated that 8-oxoguanine as a guanine oxidative damage increased dose-dependently (Fig. 1). DSB were also detected with 1 Gy-irradiation. However, the elevation of this damage was not shown with more than 1 Gy. The reason for the no increment have been still unknown. We consider that DNA repair is involved in no increase of DSB because of the low dose rate of the neutron beam.

We need further study for elucidation of molecular mechanism of neutron biological effect. The future study plan will contain the oxidative pyrimidine analysis such as 5-hydrooxycytosine. Also, the DSB will be analyzed by using of the mutant cell strains without homologous recombination (HR) and hon-homologous end joining (NHEJ). Using of these mutants leads the initial yields of DSB without DNA repair process. Additionally, we will investigate viability of the irradiated cells for concerning of DNA damage participation for neutron biological effect.

REFERENCES:

[1] H. Terato *et al.,* J. Radiat. Res., 49 (2008) 133-146.
[2] Y. Tokuyama *et al.,* J. Radiat. Res., 56 (2015) 446-455.
[3] K. Kudo *et al.,* J. Electrostat., 73 (2015) 131-139.
[4] K. Kudo *et al.,* J. Phys. D. Appl. Phys., 48 (2015) 365401.

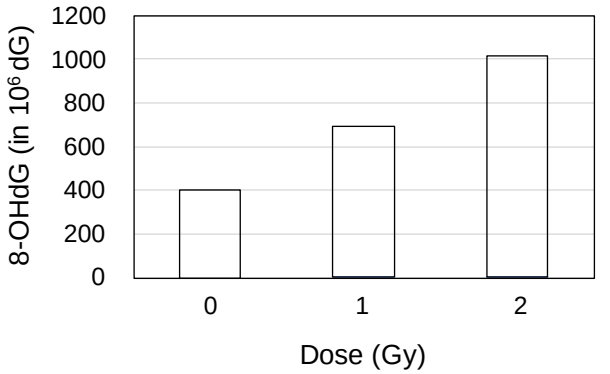

Fig. 1. Yields of 8-oxo-deoxyguanosine (8-OHdG) in the cells irradiated by the neutrons of the reactor.

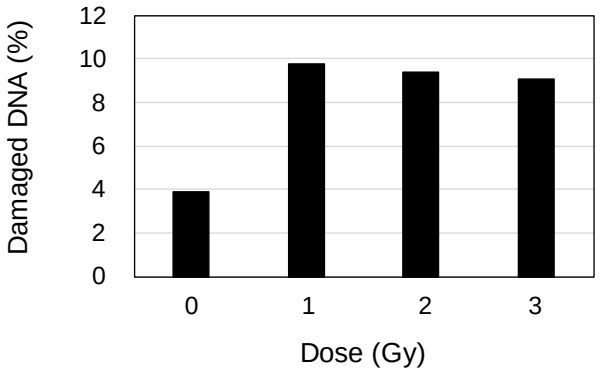

Fig. 2. Yields of DNA double strand breaks in the cells irradiated by the neutrons of the reactor.

CO1-4 Versatile Compact Neutron Diffractometer on the B–3 Beam Port of KUR

K. Mori, R. Okumura, H. Yoshino, M. Kanayama, S. Sato[1], H. Hiraka[2], K. Iwase[3], A. Okumura, and F. Kobayashi[4]

Institute for Integrated Radiation and Nuclear Science, Kyoto University (KURNS)
[1]High Energy Accelerator Research Organization (KEK)
[2]Neutron Science Center, Korea Atomic Energy Research Institute
[3]Department of Materials and Engineering, Ibaraki University
[4]Graduate School of Engineering, Kyoto University

INTRODUCTION: Neutron diffraction is a powerful tool to precisely determine the positions of light elements (e.g., hydrogen and lithium) in solids. This is the main reason why neutron powder diffractometers are critical for structural investigations of energy storage materials, for example, rechargeable lithium-ion batteries and hydrogen absorbing alloys. The B–3 beam port of Kyoto University Research Reactor (KUR) had long been used as a four-circle single-crystal neutron diffractometer (4CND). For the last decade, however, the 4CND was so old that its research activity on neutron science was quite low. Now, the versatile compact neutron diffractometer (VCND) is installed on the B-3 beam port of KUR.

SPECIFICATIONS: Fig. 1 shows the current state of the VCND. The VCND is equipped with a new beam shutter manufactured by the KURNS factory. In addition, the VCND has a wide space around the sample; therefore, we can easily install any other system. The neutron wavelength, λ, which is monochromatized by the (220) plane of a Cu single crystal (i.e., Cu monochromator), is 1 Å. To cover the detector area of $6\,° \leq 2\theta \leq 130\,°$, twenty-five ^{3}He tube detectors (1/2 inch in diameter) are used (see Fig. 2), where 2θ is the scattering angle. A detector bank including twenty-five ^{3}He tube detectors is placed on the arm of the HUBER-440 goniometer. The distance from the Cu monochromator to the sample is approximately 2 m, and the distance from the sample to the detector is 1.2 m.

CRYSTAL STRUCTURE ANALYSIS: The preliminary neutron diffraction measurements have been performed using the VCND. Fig. 3 shows the Rietveld refinement pattern of the standard sample: NIST-Si powder. As a result, an excellent fit was obtained between the observed and calculated intensities. The Bragg reflections at the high Q region (corresponding to the high 2θ region) could be observed using the VCND rather than the Laboratory X-ray diffractometer with a Cu$K\alpha$ radiation, where Q is the magnitude of the scattering vector ($= 4\pi\sin\theta/\lambda$, where θ is half of the scattering angle, 2θ). The complementary use of neutron and X-ray diffraction is very useful for the structural investigations. Further improvements are now in progress.

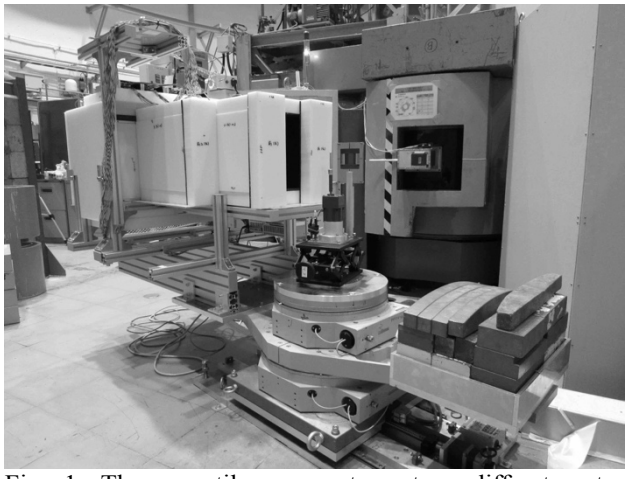

Fig. 1. The versatile compact neutron diffractometer (VCND), installed at the B-3 beam port of KUR.

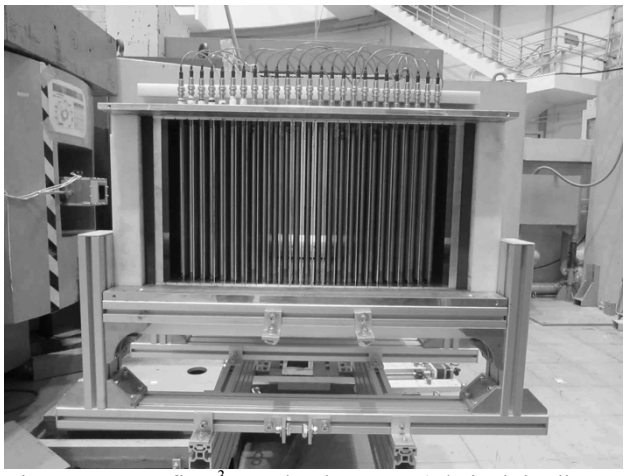

Fig. 2. Twenty-five ^{3}He tube detectors (1/2 inch in diameter) on the detector bank of the VCND.

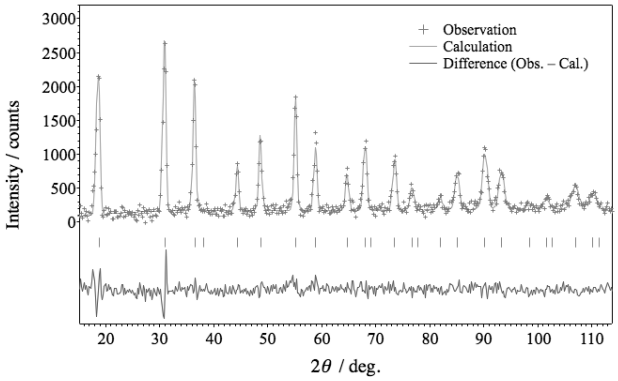

Fig. 3. The crystal structure refinement of NIST-Si using neutron diffraction data collected at the VCND.

CO1-5 Recovery Behaviors of Irradiation-Induced Defects in H_2^+-Implanted SiC and Graphite

N. Kawamura, S. Makimura, S. Matoba, J.-S. Park[1], N. Nakazato[1], H. Kishimoto[1], A. Yabuuchi[2], A. Kinomura[2] and Q. Xu[2]

Institute of Materials Structure Science, High Energy Accelerator Research Organization (KEK)
[1]Graduate School of Engineering, Muroran Institute of Technology
[2]Institute for Integrated Radiation and Nuclear Science, Kyoto University

INTRODUCTION: In J-PARC muon science experimental facility, muons are produced by irradiating a graphite target with a 3 GeV proton beam. A silicon carbide (SiC) attracts our interest for a candidate of new target material to yield more muons. Understanding tritium behavior formed in these target materials by proton irradiation is important for a stable operation in high power beam facilities like J-PARC. Macroscopic studies like TDS show that hydrogen-isotope diffusion in graphite strongly depends on the structure such as the grain size, lattice defects *etc*. Because, in the high-power beam target, the irradiation-induced vacancies are considered to trap tritiums, we investigated the recovery behavior of the vacancies using a slow positron beam.

EXPERIMENTS: 50-keV H_2^+ ions were irradiated to CVD-SiC, NITE-SiC/SiC composite [1], and graphite samples with a dose of 5×10^{16} H_2^+/cm^2. After irradiation, the samples were annealed at 500°C, 700°C, and 900°C for 15 min in N_2 atmosphere. Before and after annealing at each temperature, the samples were probed by the KUR slow positron beam and the Doppler broadening of the annihilation radiation (DBAR) spectra were acquired. The DBAR spectrum is known to be characterized by *S*- and *W*-parameters, which correlate to annihilation with low and high momentum electrons, respectively [2].

RESULTS: Figure 1 shows *S*-parameters obtained for each sample as a function of incident positron energy. They are normalized by that of each unirradiated sample annealed at 900°C. The *S*-parameter of graphite after annealing at 900°C almost recovers to the unirradiated reference-state. This is considered to be due to the recombination of the irradiation-induced vacancies and interstitials [3]. In contrast, the *S*-parameters of CVD-SiC and NITE-SiC samples show no significant change after 900°C annealing. This indicates that the irradiation-induced vacancies survive even after annealing. Figure 2 shows *S*-*W* correlations obtained for the CVD-SiC and NITE-SiC samples. If the defect specie is not changed by annealing, the *S*-*W* data should be marked on the straight line between the unirradiated state and the as-irradiated ones. However, after the annealing, the *S*-*W* points move to lower-left direction. This means that positrons are trapped at different defect species in the annealed samples, as compared to the as-irradiated ones. Although there are no significant changes in the *S*-parameters, the dominant defect species is indicated to be changed by the annealing. This result implies the defect complex of vacancies and hydrogen atoms. For further understanding, theoretical studies and electron-irradiation experiment are necessary.

ACKNOWLDGEMENTS: This study is partially supported by JSPS KAKENHI Grain Number JP16H03994.

REFERENCES:

[1] A. Kohyama *et al.*, Ceramic Transactions **256** (2016) 37.
[2] R. W. Siegel, Ann. Rev. Mater. Sci., **10** (1980) 393–425.
[3] M. Shimotomai *et al.*, J. Phys. Soc. Jpn., **52** (1983) 694–702.

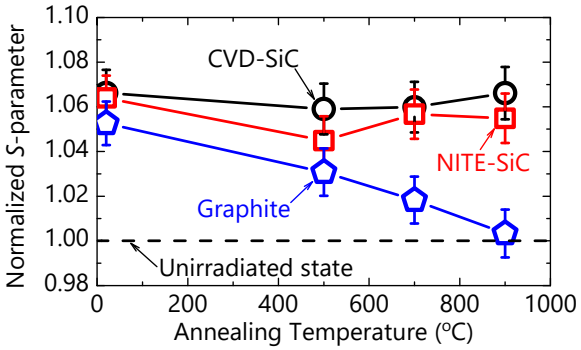

Fig. 1. *S*-parameters for CVD-SiC (open circles), NITE-SiC (open squares), and graphite (open pentagons) samples as a function of annealing temperature. Unirradiated state is also indicated as a dashed line.

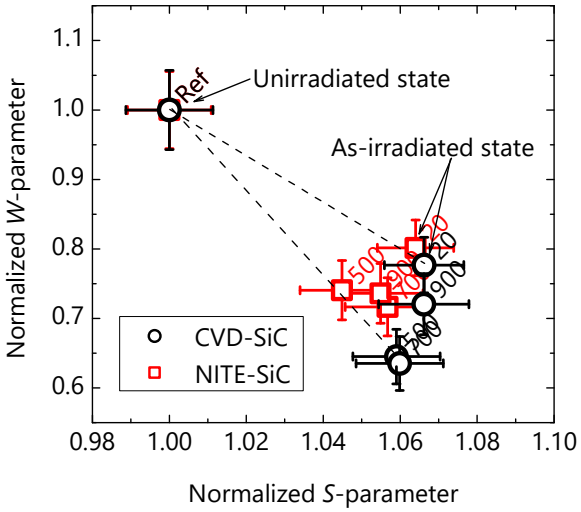

Fig. 1. *S*-*W* correlations for CVD-SiC and NITE-SiC samples. Annealing temperatures are also shown beside each symbol.

CO1-6 Measurements of thermal neutron total cross section of reactor-grade graphite

Jun Nishiyama[1], Jaehong Lee[2], Tadafumi Sano[3] and Jun-ichi Hori[2]

[1]*Laboratory for Advanced Nuclear Energy, Institute of Innovative Research, Tokyo Institute of Technology*
[2]*Institute for Integrated Radiation and Nuclear Science, Kyoto University*
[3]*Atomic Energy Research Institute, Kindai University*

INTRODUCTION: The high temperature gas-cooled reactor is a Generation IV reactor concept that use a graphite moderator. The design takes advantage of the inherent safety characteristics with specific design optimizations. The treatment of thermal scattering caused by crystalline is important for graphite to improve the prediction accuracy of graphite moderated core analysis. There is sufficient thermal scattering law for single crystal graphite, but there is no method has been established to reconstruct thermal scattering cross section for polycrystalline graphite. The differences in the scattering cross section resulting from the size of crystal grains, porosity in the graphite, and the production method of the graphite have been reported [1,2]. In order to provide basic data for thermal neutron scattering law evaluation, the total cross sections of the graphite were measured for reactor-grade graphite samples including a graphite moderator actually used in the critical assembly.

EXPERIMENTS: The total cross sections of reactor-grade graphite were measured in the incident neutron energy region from 0.001 to 10 eV by transmission experiments at the KURNS-LINAC. An experimental arrangement is shown in Fig. 1. Pulsed neutrons were produced from a water-cooled Ta-target by (γ,n) reaction with a pulsed electron beam. The incident neutron spectrum on a sample and the transmitted neutron spectrum were measured by means of a time-of-flight (TOF) method with a ^{6}Li-glass scintillation detector. A 5.0 mm diameter by 5.0 mm thick ^{6}Li-glass was located 12.0 m from the neutron source.

Two reactor-grade graphite samples were used for measurements. The characteristics of the samples are shown in Table 1. The 1/2" thickness sample is used as a moderator in the KUCA facility.

The total cross section of the graphite σ_t is calculated from the transmission spectrum and the thickness of the sample as following.

$$\sigma_t(E) = -\frac{\mathrm{A}}{\rho t N_A}\ln\big(T(E)\big) \qquad (1)$$

where ρ is the sample density, A is the atomic mass, t is the sample thickness and N_A is the Avogadro constant $T(E)$ is the transmission spectrum is derived from

$$T(E) = \frac{S(E) - A(E)}{B(E) - A(E)} \qquad (2)$$

where $B(E)$ is the incident neutron energy spectrum on the sample derived from the TOF spectrum measured with ^{6}Li-glass detector for the Blank run, $S(E)$ is the spectrum transmitted by the sample for the Sample run and $A(E)$ is the background spectrum determined by the Absorber run which performed with the polyethylene block inserted into middle of the neutron flight tube.

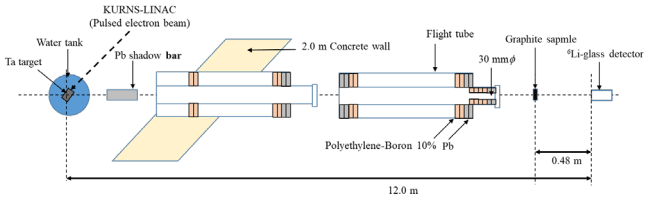

Fig 1. Experimental arrangement

Table 1 characteristics of samples

Sample	Graphite 1.0 cm	Graphite 1/2"
Crystal structure	Polycrystalline	Polycrystalline
Sample shape	Disc	Square plate
Density [g/cm^3]	1.779	1.754
Size [mm]	ϕ50	50.8×50.8
Thickness [mm]	10.0	12.7
[atoms/b]	8.92×10^{-2}	1.12×10^{-1}

RESULTS: The total cross sections of two reactor-grade graphite were derived in the incident neutron energy region from 0.001 to 10 eV. The present results are shown in Fig. 2. A clear first black edge was observed at 0.0018 eV for both samples. In the energy range of 0.1 eV or more, the results are good agreement within the error, but there is discrepancy in the energy region 0.0018 to 0.02 eV.

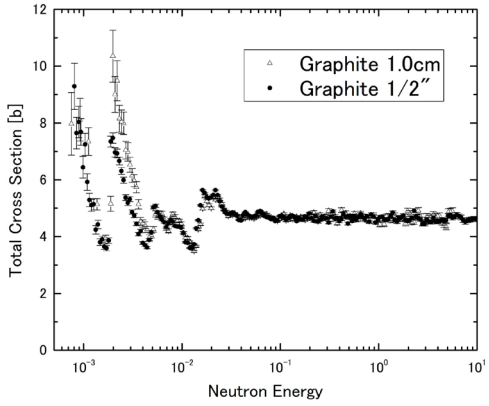

Fig. 2 Total cross section of graphite

REFERENCES:

[1] C. D. Bowman *et al.*, Nucl. Sci. Eng., **159** (2008) 182-198.
[2] S. Petriw *et al.*, J. Nucl. Materials., **396** (2010) 181-188.

CO1-7 Development of neutron spin flipper with large beam acceptance

M. Kitaguchi, H. Okabe[1], T. Oda[2], and M. Hino[2]

Center for Experimental Studies, KMI, Nagoya University
[1]Department of Physics, Nagoya University
[2]Institute for Integrated Radiation and Nuclear Science, Kyoto University

INTRODUCTION: The recent values of neutron lifetime deviate far beyond the systematic errors claimed in the past and require the further improvement for the neutron the lifetime puzzle. We are continuing neutron lifetime measurement at the polarized beam branch of the NOP beamline installed at the port BL05. The system consists of a neutron chopper (SFC) and a gas chamber (TPC) for detecting the electrons from the neutron beta decays. The TPC contains small amount of ^{3}He. The rate of the ^{3}He(n,p)^{3}H reaction is measured by counting the protons. The neutron lifetime is measured as the ratio of the electron events to the proton events [1].
The large background via neutron-induced reactions is suppressed by introducing small neutron bunches into the TPC and selectively detecting decay electrons and reaction protons only when neutron bunches are traveling inside the sensitive volume and they were not transmitting through chamber windows and other materials on the beam path. The SFC is a spin-selective optics to switch the neutron beam using the combination of magnetic supermirrors and spin flippers[2]. Polarized neutrons are injected into the SFC. Controlling the timing of spin-flip makes neutron bunches at the exit of the SFC, which can be reflected by the magnetic mirrors successively. By employing the triple series reflection, the present version of the SFC chops the neutron beam with the intensity contrast of about 400. During the lifetime measurement, the bunch length is adjusted as about 50 cm, which is half of the length of TPC sensitive region for maximizing the signal statistics. The cross section of the output bunches is 2 cm ×2 cm. In order to reduce the statistical uncertainties for the lifetime measurement to the order of 1 s, the incident neutron flux into the TPC must be increased. Although the new mirrors have been already assembled to accept large cross section of the neutron beam, large scale of spin flippers are also required. Now we are also continuing to develop the precision simulation of neutron spin behavior. Numbers of spin flippers, which have various performances, should be investigated and compared with the simulations.

EXPERIMENTS: The experiments were performed at cold neutron beamline CN3 in KUR. Figure 1 shows the experimental setup. Disk chopper provided pulsed neutrons. Magnetic supermirrors were used for neutron polarizer and analyzer. The position and time-of-flight from the chopper to the detector were measured. The behavior of the spin of each neutron was investigated by scanning the position and magnetic field of the flipper coil.

RESULTS: The dependence of spin flipping probability not only for neutron wavelength but also for the position of the flipper coil was observed clearly. It means that the position distribution of the magnetic field of the coil may have non-negligible influences of the spin behavior. This can be reproduced numerically by our simulation (Fig. 2). New flipper coils with large beam acceptance are developed by using the simulation-based design.

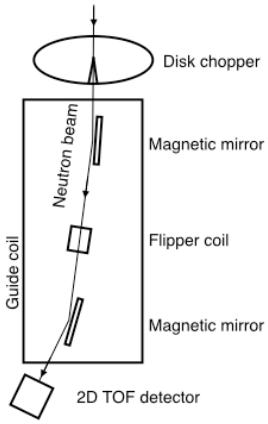

Fig. 1. Experimental setup with polarized neutron beam at CN3 beamline.

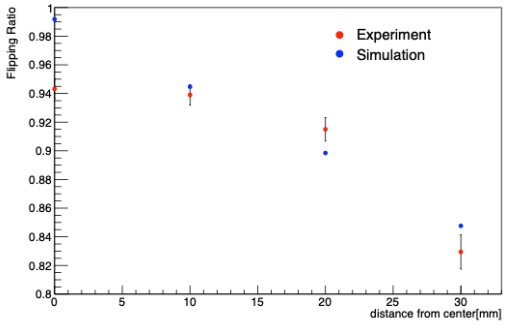

Fig. 2. Position dependence of spin flipping ratio in the flipper coil.

REFERENCES:
[1] K. Mishima *et al.,* Nucl. Instr. and Meth., A600 (2009) 342.
[2] K. Taketani *et al.*, Nucl. Instr. and Meth., A634 (2011) S134–S137.

CO1-8 Development of high spatial resolution cold/ultracold neutron detector using nuclear emulsion

N. Naganawa, M. Hino[1], K. Hirota[2], H. Kawahara[2], M. Kitaguchi[3], K. Mishima[4], N. Muto[2], Y. Seki[5], S. Tada[2], A. Umemoto[2]

Institute of Materials and Systems for Sustainability, Nagoya University

[1]*KURNS, Kyoto University*

[2]*Graduate School of Science, Nagoya University*

[3]*Kobayashi-Maskawa Institute for the Origin of Particles and the Universe*

[4]*High Energy Accelerator Research Organization, KEK*

[5]*Japan Proton Accelerator Research Complex*

INTRODUCTION: We have been developing a high spatial resolution neutron detector using fine-grained nuclear emulsion[1] and a thin converter layer including ^{10}B for measurements of position distributions of cold and ultracold neutrons such as the one of quantized ultracold neutrons under the earth's gravitational field[2]. The detector will also be useful for neutron imaging. In a previous study, we confirmed it having a spatial resolution of less than 100 nm for the one with its converter ($^{10}B_4C$) thickness of 50 nm[3]. In this study, we increased the thickness to 200 nm to increase its detection efficiency with keeping its resolution. It was fabricated by the ion beam sputtering system of KURRI (KUR-IBS). Its detection efficiency of neutrons was measured at CN-3 beamline. Next, also detectors with converter thickness of 2 μm was fabricated and its ability to record microscopic patterns was demonstrated using absorption gratings made of Gd. Exposure experiments was carried out at CN-3 and BL05 of MLF, J-PARC.

EXPERIMENT 1: A converter layer of $^{10}B_4C$ (200 nm)-NiC (60 nm)-C (20 nm) was fabricated by KUR-IBS on a 0.38 mm-thick Si plate. It was coated with 10 μm-thick fine-grained emulsion. Finally, it was covered with two foils of 10 μm-thick aluminum to avoid light. It was exposed to neutrons with typical wavelength of 2.4 Å at CN-3 at the downstream of a 3 mm-diameter pinhole made by Cd. The exposure density of neutrons was 7.36×10^7 n/cm^2. After the exposure, the detector was developed at Nagoya University. Track of α-particles and ^{7}Li nuclei from absorptions were recorded in it was counted manually under an epi-illumination optical microscope.

RESULTS:

A total of 30±5 tracks were found in a view of the microscope whose area is 100 μm×100 μm. Horizontal tracks were not counted for separation from scratch marks on the Si plate. Since a number of neutrons arrived at the area was 7.36×10^4, its detection efficiency turned out to be (0.40±0.07)% for the neutrons of the beam.

EXPERIMENT 2.1: To demonstrate the ability to record microscopic position distributions of neutrons, our detector was exposed to neutrons at CN-3 at the downstream of an absorption grating made of Gd which has apertures of 3 μm wide with a period of 9 μm[4]. In this experiment, a detector with a converter layer of $^{10}B_4C$ (2 μm)-NiC (60 nm)-C (20 nm) was fabricated by IBS-KUR, then coated with the emulsion at Nagoya University. The distance between the grating and the detector was 1.5 mm. They were exposed to neutrons with typical wavelength of 2.4 Å with divergence of ±5 mrad just at the downstream of the guide pipe up to 7×10^{10} n/cm^2. A blur of the neutron image due to the divergence of the beam was assumed to be 7 μm. After development, an image was taken under the microscope with a CMOS camera.

RESULTS: As shown in Fig. 1, a microscopic pattern of the grating was obtained consistently with the dimension of blur due to the beam setting.

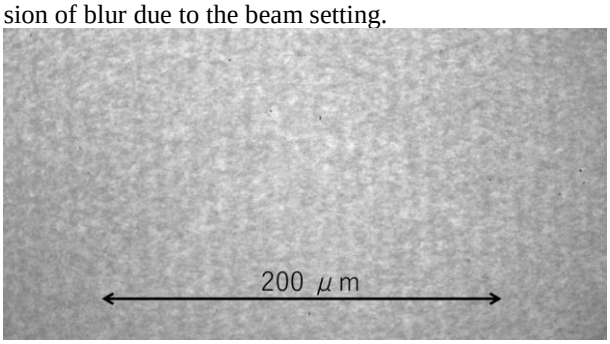

Fig. 1. A neutron image taken by a detector with a 2 μm-thick $^{10}B_4C$ layer at 1.5 mm downstream of the grating with a beam divergence of ±5 mrad. Dark part in the view consists of tracks from absorptions.

EXPERIMENT 2.2: In order to obtain a clearer image, a similar exposure was done at the Low Divergence Beam Line of BL05 in MLF, J-PARC. Another piece of the same detector as EXPERIMENT 2.1 was exposed to 4 Å neutrons with divergence of ±0.056 mrad at 900 μm downstream of the same kind of slit. The amount of neutrons which it was exposed to was 8.2×10^8 n/cm^2. A blur was assumed to be 50 nm.

RESULTS: As shown in Fig. 2, a clear microscopic pattern of the grating was seen.

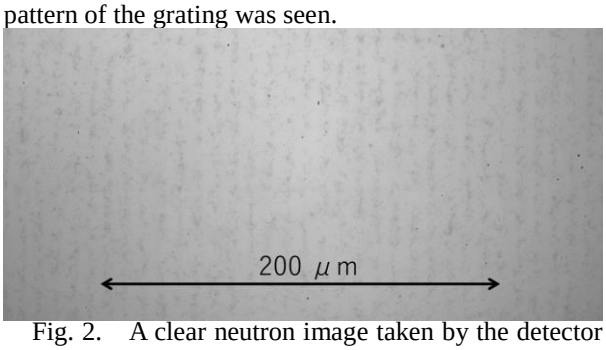

Fig. 2. A clear neutron image taken by the detector at 900 μm downstream of the grating with a beam divergence of ±0.056 mrad.

REFERENCES:

[1] T. Asada *et al,,* Prog. Thor. Exp. Phys., 2017 (2017) 063H01.

[2] V. V. Nesvizhevsky *et al.,* Nature,415 (2002) 297.

[3] N. Naganawa *et al.,* Eur. Phys. J. C, 78(2018)959.

[4] Y. Seki *et al.,* Physics Procedia 88 (2017) 217–223.